Elucidate the Formation Mechanism of Particulate Nitrate Based on Direct Radical Observations in the Yangtze River Delta summer 2019

Tianyu Zhai[a], Keding Lu[a, b], Haichao Wang[c], Shengrong Lou[d], Xiaorui Chen[a, f], Renzhi Hu[e], Yuanhang Zhang[a, b*]*

[a] State Key Joint Laboratory of Environmental Simulation and Pollution Control, College of Environmental Sciences and Engineering, Peking University, Beijing 100871, China.

[b] Collaborative Innovation Center of Atmospheric Environment and Equipment Technology, Nanjing University of Information Science & Technology, Nanjing 210044, China.

[c] School of Atmospheric Sciences, Sun Yat-sen University, Guangzhou 510275, China.

[d] State Environmental Protection Key Laboratory of Formation and Prevention of the Urban Air Complex, Shanghai Academy of Environmental Sciences, Shanghai, 200223, China.

[e] Key Laboratory of Environmental Optics and Technology, Anhui Institute of Optics and Fine Mechanics, Chinese Academy of Sciences, Hefei, 230031, China.

[f] Now at: Department of Civil and Environmental Engineering, The Hong Kong Polytechnic University, Hong Kong, China.

Correspondence to:

Keding Lu (k.lu@pku.edu.cn), Yuanhang Zhang (yhzhang@pku.edu.cn)

24   **Abstract.** Particulate nitrate (NO_3^-) is one of the dominant components of fine particles

25   in China, especially during pollution episodes, and has a significant impact on human

26   health, air quality, and climate. Here a comprehensive field campaign that focuses on

27   the atmospheric oxidation capacity and aerosol formation and their effects in the

28   Yangtze River Delta (YRD) was conducted from May to June 2019 at a regional site in

29   Changzhou, Jiangsu province in China. The concentration of NO_3^-, OH radical, N_2O_5,

30   NO_2, O_3, and relevant parameters were measured simultaneously. We showed a high

31   NO_3^- mass concentration with $10.6 \pm 8.9 \, \mu g \, m^{-3}$ on average, which accounted for 38.3 %

32   of total water-soluble particulate components and 32.0 % of total $PM_{2.5}$, followed by

33   the proportion of sulfate, ammonium, and chloride by 26.0 %, 18.0 %, and 2.0 %,

34   respectively. This result confirmed that the heavy nitrate pollution in eastern China not

35   only happened in winter but also in the summertime. This study's high nitrate oxidation

36   ratio (NOR) emphasizes the solid atmospheric oxidation and fast nitrate formation

37   capacity in YRD. It is found that $OH + NO_2$ during daytime dominates nitrate formation

38   on clean days while N_2O_5 hydrolysis vastly enhanced and became comparable with that

39   of $OH + NO_2$ during polluted days (67.2 % and 30.2 %, respectively). An updated

40   observed-constrain Empirical Kinetic Modeling Approach (EKMA) was used to assess

41   the kinetic controlling factors of both local O_3 and NO_3^- productions, which indicated

42   that the O_3-targeted scheme (VOCs: NO_x = 2: 1) is adequate to mitigate the O_3 and

43   nitrate pollution coordinately during summertime in this region. Our results promote

44   the understanding of nitrate pollution mechanisms and mitigation based on field

45   observation and model simulation and call for more attention to nitrate pollution in the

46   summertime.

47   **Keywords:**

48   Nitrate pollution; Dinitrogen pentoxide; Nitrate formation; Pollution mitigation

1 Introduction

Chemical compositions of fine particles have been measured in China during the past twenty years, and secondary inorganic aerosol is regarded as one of the dominant species in aerosol (Cao et al., 2012; Hagler et al., 2006; Zhao et al., 2013; Andreae et al., 2008). Since the Air Pollution Prevention and Control Action Plan, there has been a significant decrease in SO_2, NO_2, and $PM_{2.5}$ concentration in China, while the inorganic nitrate ratio in $PM_{2.5}$ increased and became the considerable component in $PM_{2.5}$ (Shang et al., 2021; Zhang et al., 2022). Therefore, a comprehensive understanding of the particlate nitrate formation mechanism is essential and critical to mitigating haze pollution in China.

Massive research has been done in China to investigate nitrate formation mechanisms, and a basic framework has been established (Sun et al., 2006; Chang et al., 2018; Wu et al., 2019). In the daytime, $NO_2 + OH$ radical oxidation (Reaction 1) is the major particulate nitrate formation pathway. The product (HNO_3) reacts with alkaline substances in aerosol, generating particulate nitrate. This pathway is mainly controlled by precursors concentration as well as the gas-particle partition of gaseous nitric acid, and particulate nitrate depends on temperature, relative humidity (RH), NH_3 concentration, and aerosol acidity (Wang et al., 2009; Song and Carmichael, 2001; Meng et al., 2020; Zhang et al., 2021). At night, N_2O_5 uptake is a vital nitrate formation pathway (Reaction 4)(Chen et al., 2020; Wang et al., 2022). N_2O_5 is formed through $NO_2 + NO_3$ (Reaction 3) and there exists a quick thermal equilibrium balance ($K_{eq} = 5.5 \times 10^{-17}$ cm^{-3} molecule^{-1} s^{-1}, 298 K). However, two problems remain ambiguous in quantifying the contribution of N_2O_5 uptake to nitrate formation. The first is the N_2O_5 heterogeneous uptake coefficient (γ) on ambient aerosol is highly varied with the range from 10^{-4} to 10^{-1} based on previous lab and field measurements (Bertram and Thornton, 2009; Brown et al., 2009; Wang et al., 2017c; Wang and Lu, 2016). The other one is $ClNO_2$ production yield which influences nitrate contribution due to the extensive variation range (Phillips et al., 2016; Staudt et al., 2019; Tham et al., 2018). Both two

77 parameters are complex to well-predicted by current schemes. NO_2 heterogeneous

78 uptake has been found nonnegligible for nitrate formation, which can be a vital pathway

79 during heavy haze events, according to recent study (Qiu et al., 2019; Chan et al., 2021).

80 The uptake coefficient and nitrate yield remain uncertain, as same as the N_2O_5

81 heterogeneous reaction. Besides, N_2O_5 homogeneous hydrolysis and NO_3 radical

82 oxidation have a minor contribution to particulate nitrate under ambient conditions

83 (Brown et al., 2009; Seinfeld and Pandis, 2016).

$$NO_2 + OH \rightarrow HNO_3 \qquad\qquad R1$$

$$NO_2 + O_3 \rightarrow NO_3 + O_2 \qquad\qquad R2$$

$$NO_2 + NO_3 + M \rightarrow N_2O_5 + M \qquad\qquad R3.1$$

$$N_2O_5 + M \rightarrow NO_2 + NO_3 + M \qquad\qquad R3.2$$

$$N_2O_5 + (H_2O \text{ or } Cl^-) \rightarrow (2 - \varphi) NO_3^- + \varphi ClNO_2 \qquad\qquad R4$$
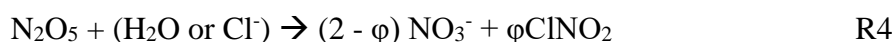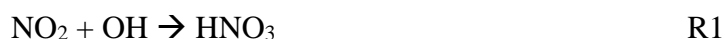
84 As a critical area of China's economy and industry, Yangtze River Delta (YRD)

85 has suffered severe air pollution during past decades, and fine particle pollution in YRD

86 has raised a widespread concern (Guo et al., 2014; Zhang et al., 2015; Zhang et al.,

87 2017; Ming et al., 2017; Xue et al., 2019). However, most research focuses on

88 wintertime $PM_{2.5}$ pollution and lacks measurements of critical intermediate species and

89 radicals to assess the importance of each nitrate formation pathway. In this study, with

90 the direct measurements of hydroxyl radical and the reactive nitrogen compounds and

91 chemical box model analysis, we explore the characteristics of nitrate and precursors in

92 YRD in the summer of 2019, the importance of particulate nitrate formation pathways

93 is quantified, and the controlling factors are explored. A further suggestion for summer

94 pollution prevention and control in the local area is proposed.

2 Site description and methods

2.1 The campaign site

This campaign took place at a suburban sanatorium from May 30th to June 18th, 2019, in Changzhou, China. Changzhou (119.95 °E, 31.79 °N) is located in Jiangsu province and about 150 km northwest of Shanghai. The sanatorium, located 420 m east of Lake Ge (one of the largest lakes in Jiangsu province, 164 square kilometers), is surrounded by farmland and fishponds. With the closest arterial traffic 1 km away, several industry zones are 4 km to the east. The prevailing wind was from the south and southeast sectors (about 30 % of the time) compared to 20 % from the west sector, of which only 15 % came from the east. The wind speed was usually lower than 5 m s^{-1} with faster speed from the west. This site was influenced by anthropogenic and biological sources with occasional biomass burning.
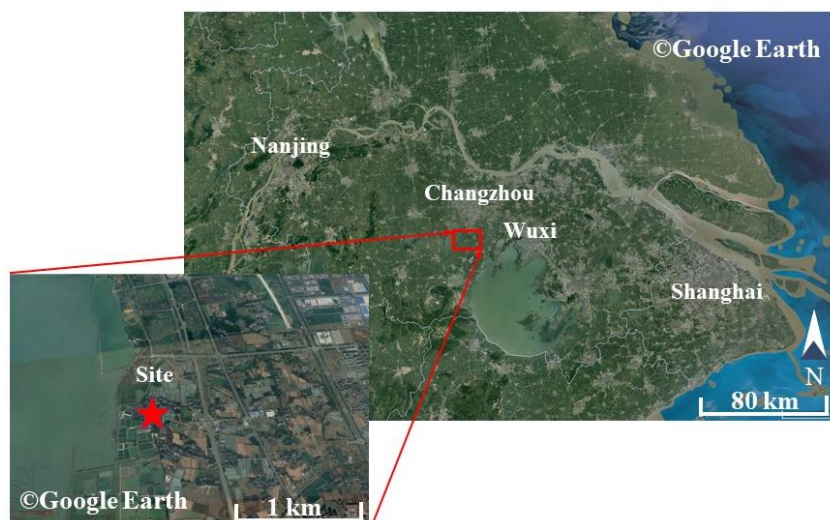
Figure 1 The location of the campaign site (red star), Changzhou, is 150 km on the northwest side of Shanghai.

2.2 The instrumentation

Multiple gaseous and particlate parameters were measured simultaneously during the

112   campaign to comprehensively interpret the nocturnal atmospheric capacity and aerosol

113   formation. The related instruments are listed in Table 1. N_2O_5 and Particle Number and

114   Size Distribution (PNSD) were measured on the fourth floor of the sanatorium, which

115   is the top of the building. Other instruments were placed in containers on the ground

116   170 m northeast of the building and sampling inlets at circa 5 m above the ground

117   through the containers' roof.

118   N_2O_5 was measured by Cavity Enhanced Absorption Spectrometer (CEAS) based

119   on Lambert-Beer's law which was developed by (Wang et al., 2017b). Briefly, air

120   samples were drawn through the window and reached out of the wall 30 cm to prevent

121   influence from surface deposition. The aerosol membrane filter was deployed before

122   the PFA sampling tube and changed every 2 hours at night to avoid a decrease in N_2O_5

123   transmission efficiency due to the increased loss of N_2O_5 from the accumulated aerosols

124   on the filter. N_2O_5 was decomposed to NO_3 and NO_2 through preheating tube heat at

125   130 ℃ and detected within a PFA-coated resonator cavity heated at 110 ℃ to prevent

126   the formation of N_2O_5 by reversible reaction subsequently. At the end of each sampling

127   cycle (5 min), a 30 s injection of high concentration NO (10 ppm, 20 ml min^{-1}) mixed

128   with sample air was set to eliminate NO_3-N_2O_5 in the system. The NO titration

129   spectrums were adopted as the dynamic background spectrum by assuming no H_2O

130   concentration variation in a single sampling cycle. The loss of N_2O_5 in the sampling

131   system and filter was also considered during data correction. The limit of detection

132   (LOD) was estimated to be 2.7 pptv (1 σ) with an uncertainty of 19 %.

133   OH radical measurement was conducted by Fluorescence Assay by Gas Expansion

134   Laser-Induced Fluorescence techniques (FAGE-LIF). Ambient air was expanded

135   through a 0.4 mm nozzle to low pressure in a detection chamber, where the 308 nm

136   laser pulse irradiated OH radical at a repetition rate of 8.5 kHz (Chen et al., 2018). NO_x

137   and O_3 were monitored by commercial monitors (Thermo-Fisher 42i and 49i). Volatile

138   organic compounds (VOCs) were measured by an automated Gas Chromatograph

139   equipped with a Mass Spectrometer and flame ionization detector (GC-MS) with a time

140 resolution of 60 min. The photolysis frequencies were determined from the spectral

141 actinic photon flux density measured by a spectroradiometer (Bohn et al., 2008).

142     $PM_{2.5}$ concentration was obtained by Tapered Element Oscillating Microbalance

143 (TEOM 1405, Thermo Scientific Inc). Aerosol surface concentration (S_a) was

144 converted from particle number and size distribution, which was measured by Scanning

145 Mobility Particle Sizer (SMPS, TSI 3936) and Aerosol Particle Sizer (APS, TSI 3321)

146 and modified to the wet particle-state S_a with a hygroscopic growth factor (Liu et al.,

147 2013). The uncertainty of the wet S_a was ~ 30 %. Meanwhile, water-soluble particulate

148 components and their gaseous precursors were analyzed through the Monitor for

149 AeRosols and GAses in ambient air (MARGA, Chen et al. (2017)). Meteorological data

150 were also available, including the temperature, relative humidity (RH), pressure, wind

151 speed, and wind direction.

152 **Table 1** The observed gas and particle parameters during the campaign.

Parameters	Detection of limit	Method	Accuracy
N_2O_5	2.7 pptv (1 σ, 1 min)	CEAS	± 19 %
OH	1.6×10^5 cm^{-3} (1 σ, 60 s)	LIF[a]	± 21 %
NO	60 pptv (2 σ, 1 min)	PC[c]	± 10 %
NO_2	0.3 ppbv (2 σ, 1 min)	PC[c]	± 10 %
O_3	0.5 ppbv (2 σ, 1 min)	UV photometry	± 5 %
VOCs	20-300 pptv (60 min)	GC-MS	± 15 %
$PM_{2.5}$	0.1 μg m^{-3} (1 min)	TEOM[d]	± 5 %
Photolysis frequencies	5×10^{-5} s^{-1} (1 min)	SR[e]	± 10 %
PNSD	14 nm -700 nm (4 min)	SMPS, APS	± 10 %
HNO_3, NO_3, HCl	0.06 ppbv (30 min)	MARGA[f]	± 20 %
NH_4^+, NO_3^-, Cl$^-$, SO_4^{2-}	0.05 μg m^{-3} (30 min)	MARGA[f]	± 20 %

153 [a] Laser-induced fluorescence; [b] Chemiluminescence; [c] Photolytic converter; [d] Tapered

154 Element Oscillating Microbalance; [e] Spectroradiometer; [f] the Monitor for AeRosols and

155 GAses in ambient air.

2.3 The empirical kinetic modeling approach

157 A box model coupled with the Regional Atmospheric Chemical Mechanism version 2

158 (RACM2, Goliff, Stockwell & Lawson, 2013) is used to conduct the mitigation

159 strategies studies. The model is operated in one-hour time resolution with measurement

160   results of temperature, relative humidity, pressure, CO, NO$_2$, H$_2$O, photolysis

161   frequencies, and aggregated VOCs input to constrain the model. It should be noted that

162   HONO concentration is calculated by NO$_2$ times 0.02, as suggested by Elshorbany et al.

163   (2012), and has been used in the box model before (Lou et al., 2022). Long-lived species

164   such as H$_2$ and CH$_4$ are assumed as constants (550 ppbv and 1900 ppbv, respectively).

165   Moreover, a 13-hour constant loss rate of unconstrained intermediate and secondary

166   products, the result of synthetic evaluating secondary simulation of secondary species,

167   is set for representing the multi-effects of deposition, transformation, and transportation.

168   The approaches to the chemical production of O$_3$ (P(O$_3$)) and inorganic nitrate

169   (P(NO$_3^-$)) are described in previous articles (Tan et al., 2021; Tan et al., 2018) and

170   expressed as Equation 1 and 4:

$$P(O_3) = F(O_3) - D(O_3) \qquad \text{Eq1}$$

$$F(O_3) = k_{HO_2+NO}[NO][HO_2] + k_{(RO_2+NO)eff}[NO][RO_2] \qquad \text{Eq2}$$

$$D(O_3) = k_{OH+NO_2}[OH][NO_2] + (k_{OH+O_3}[OH] + k_{HO_2+O_3}[HO_2] + k_{alkenes+O_3}[alkenes])[O_3] \qquad \text{Eq3}$$

$$P(NO_3^-) = P(HNO_3) + P(pNO_3^-) \qquad \text{Eq4}$$

$$P(HNO_3) = k_{OH+NO_2}[OH][NO_2] \qquad \text{Eq5}$$

$$P(pNO_3^-) = 0.25(2 - \varphi)\, C\, \gamma\, S_a\, [N_2O_5] \qquad \text{Eq6}$$

171   briefly, P(O$_3$) is net ozone production, which is calculated by peroxyl radial + NO

172   oxidation (Eq. 2) minus the chemical loss of O$_3$ and NO$_2$ (Eq. 3). P(NO$_3^-$) is constituted

173   by reaction OH + NO$_2$ (Eq. 5) and N$_2$O$_5$ heterogeneous uptake (Eq. 6). Here, rate

174   constants of reactions are obtained from NASA JPL Publication (Burkholder et al.,

175   2015) or RACM2 (Goliff et al., 2013). γ is the N$_2$O$_5$ uptake coefficient calculated from

176   parameterization (γ_P, more details in chapter 3.3). φ represents ClNO$_2$ production yield

177   through N$_2$O$_5$ hydrolysis, and the mean value reported by Xia et al. (2020) is used in

178   this work.

179   The empirical Kinetic Modeling Approach (EKMA) was innovated to study the

180   effects of precursors (VOCs and NO$_x$) reactivity on the region's ozone pollution by

181   Kanaya et al., which helps recognize the region's susceptibility to precursors by weight

182   and become a prevalent tool to study the process of ozone formation (Tan et al., 2018;

183   Yu et al., 2020b; Kanaya et al., 2008). The prevention and control problem of pollutant

184   generation can be transformed through the EKMA curve to reduce its precursors'

185   emissions. Furthermore, the precursor reduction scheme needed for total pollutant

186   control is given qualitatively. P(NO$_3^-$) can also be analyzed through EKMA for the

187 nonlinear secondary formation relationship with precursor reactivity. Here, an isopleth

188 diagram of the net ozone production rate as functions of the reactivities of NO_x and

189 VOCs can be derived from EKMA. In detail, 0.01 to 1.2 emission reduction strategy

190 assumptions are exponential interpolation into 20 kinds of emission situations of NO_x

191 and VOCs, respectively, which in total counts 400 scenarios.

192 **2.4 The calculation of aerosol liquid water content**

193 Aerosol liquid water content (ALWC) is calculated through ISORROPIA II

194 (Fountoukis and Nenes, 2007). Forward mode is applied in this study. Furthermore,

195 water-soluble particulate components in $PM_{2.5}$ and gaseous species ($NH_3 + HNO_3 + HCl$)

196 obtained from MARGA, along with RH and T, are input as initial input. In addition,

197 metastable aerosol state is chosen due to high RH during this campaign.

198 **3 Result and discussion**

199 **3.1 Overview of measurements**

200 The time used in this study is China Standard Time (UTC + 8) and the local sunrise and

201 sunset time during the campaign were around 5 am and 7 pm, respectively. The whole

202 campaign period is divided into four $PM_{2.5}$ clean periods and four $PM_{2.5}$ polluted

203 periods (9 out of 14 days, the latter polluted periods days day refer to $PM_{2.5}$ pollution

204 except specified description) according to the Chinese National Air Quality Standard

205 (CNAAQS) Grade I of daily $PM_{2.5}$ concentrations (< 35.0 μg m^{-3}). Figure 2 shows the

206 meteorological parameters, and gas-phase and particulate species timeseries during the

207 observation. During the campaign, the temperature was high; the maximum reached

208 34.5 °C, with an average of 25.1 ± 3.7 °C. RH changed drastically from 21 % to 88 %,

209 with a mean value of 58.9 ± 14.0 %. The mean NO_2 concentration was 14.8 ± 9.5 ppbv.

210 Meanwhile, the O_3 average was 54.6 ± 28.8 ppbv, exceeding CNAAQS Grade II for a

211 maximum daily average of 8 h ozone (160 μg m^{-3}) on 14 out of 19 days and exceeding

212 200 μg m^{-3} on six days.
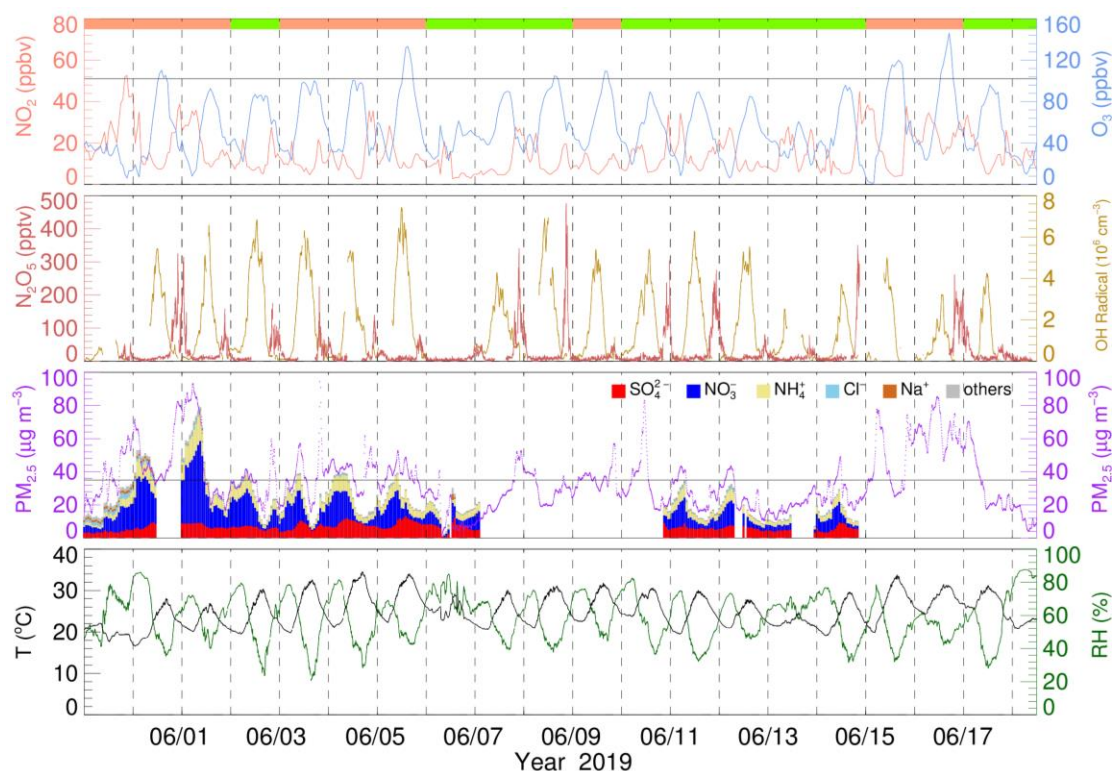
213

214 **Figure 2** Timeseries of NO_2, O_3, N_2O_5, OH radical, $PM_{2.5}$, and water-soluble particulate

215 components, temperature, and RH. The vertical dotted line represents the zero clock.

216 The black horizontal solid line in O_3 and $PM_{2.5}$ panels represents Chinese national air

217 quality standards for O_3 and $PM_{2.5}$, respectively. The top panel color blocks represent

218 the $PM_{2.5}$ clean day (light green) and $PM_{2.5}$ polluted day(salmon).

219

220 Daytime OH radical ranged from 2×10^6 to 8×10^6 molecular cm^{-3} with a daily

221 peak over 3×10^6 molecular cm^{-3}. Maximum OH radical reached 8.18×10^6 molecular

222 cm^{-3} in this campaign. Compared with other summertime OH radical observed in China,

223 OH radical concentration in this site is relatively low but still on the same order of

224 magnitude (Lu et al., 2012; Lu et al., 2013; Ma et al., 2022; Tan et al., 2017; Woodward-

225 Massey et al., 2020; Yang et al., 2021). N_2O_5 mean concentration was 21.9 ± 39.8 pptv

226 with a nocturnal average of 61.0 ± 63.1 pptv and a daily maximum of over 200 pptv at

227 eight nights. The maximum concentration of N_2O_5 (477.2 pptv, 5 min resolution)

228 appeared at 20:47 on June 8th. The average NO_3 radical production rate $P(NO_3)$ is 2.1

229 $\pm$ 1.4 ppbv h^{-1} with nocturnal average $P(NO_3)$ 2.8 ± 1.6 ppbv h^{-1} and daytime $P(NO_3)$

230 2.2 ± 1.4 ppbv h^{-1}. $P(NO_3)$ is about twice of documented value in Taizhou and North

231 China Plain (Wang et al., 2017a; Wang et al., 2018b; Wang et al., 2020a), but close to

232   another result in YRD before (Chen et al., 2019). The average $PM_{2.5}$ was 34.6 ± 17.8

233    $\mu g\ m^{-3}$ with a maximum reach of 163.0 $\mu g\ m^{-3}$. The water-soluble particulate

234   components of $PM_{2.5}$ are displayed as well. The average NO_3^- concentration was 10.6

235    $\mu g\ m^{-3}$, which accounts for 38.3 % mass concentration of water-soluble particulate

236   components and 32.0 % total $PM_{2.5}$, while the proportion of sulfate, ammonium, and

237   chloride is 26.0 %, 18 %, and 2.0 % respectively. To sum up, during the campaign

238   period, the pollution of $PM_{2.5}$ would be generally exacerbated on high O_3 and NO_2 days.

239   Precipitation occurred during four clean processes receded pollutant concentration;

240   otherwise, the pollution condition remained severe.

241   The mean diurnal variations (MDC) of temperature, RH, NO_2, O_3, $P(NO_3)$, N_2O_5,

242   OH radical, and $PM_{2.5}$ in different air quality are shown in Figure 3. The temperature,

243   RH, and OH radical MDC show indistinctive differences between clean days (CD) and

244   polluted days (PD). The MDC of NO_2 has two concentration peaks that appear at 06:00

245   and 21:00 on CD, while at PD, its peak appears at 20:00 and maintains a high level

246   during the whole night. O_3 diurnal pattern reflects a typical urban-influenced character

247   with a maximum O_3 peak that lasts four hours from 14:00 to 17:00, while polluted-day

248   O_3 peak concentration is 1.2 higher than clean-day. $P(NO_3)$ grows after the O_3 peak and

249   maximum $P(NO_3)$ shows at 19:00 with an average value of 1.7 ppbv h^{-1} on CD. By

250   contrast, the mean polluted-day P(NO3) is 2.6 ppbv h-1, and the maximum value

251   reaches 4.7 ppbv h^{-1}. In contrast, the clean-day N_2O_5 has a higher average and maximum

252   concentration than PD, which suggests a faster removal process during PD. $PM_{2.5}$ has

253   a similar trend with $P(NO_3)$ and has a higher concentration during nighttime.

254
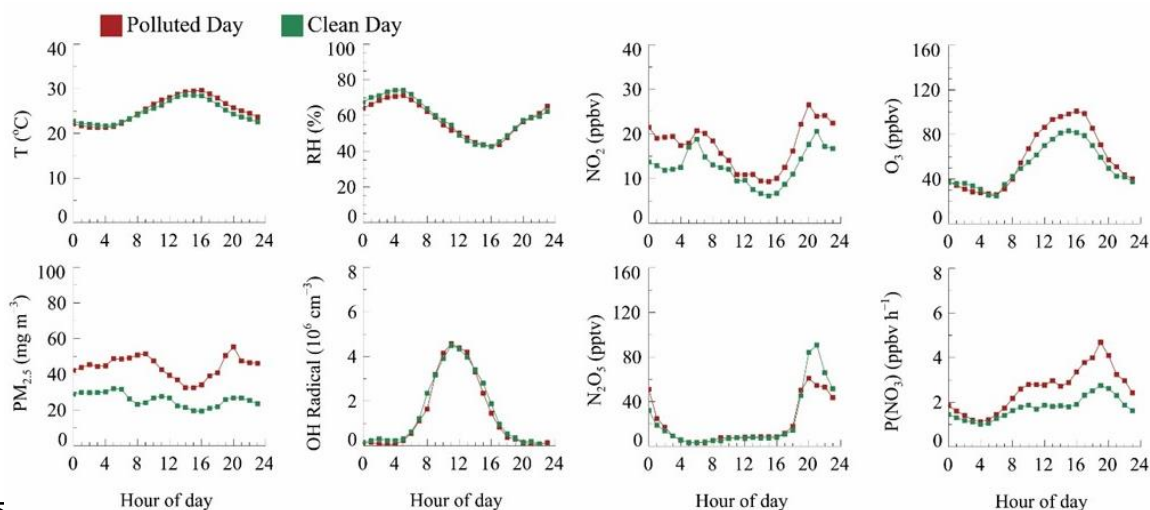
255

256 **Figure 3** The mean diurnal variations of temperature, RH, NO_2 (Salmon), O_3, $P(NO_3)$,

257 N_2O_5, OH radical(orange), and $PM_{2.5}$ of clean day and polluted day.

3.2 The evolution of nitrate pollution

259 Figure 4 (a) shows the relationship between nitrate and sulfate with water-soluble

260 particulate components. Nitrate positively correlates with total water-soluble

261 particulate components, while the sulfate ratio has an inverse correlation. With $PM_{2.5}$

262 concentration increasing, nitrate proportion increases rapidly and keeps high weight at

263 heavy $PM_{2.5}$ period while sulfate ratio pears opposite phenomenon. Once the mass

264 concentration of total water-soluble particulate component is over 30 μg m^{-3}, the mass

265 fraction of nitrate in total water-soluble particulate components is up to 50 % on average.

266 This result illustrates that particulate nitrate is one of the vital sources of explosive

267 growth particulate matter.
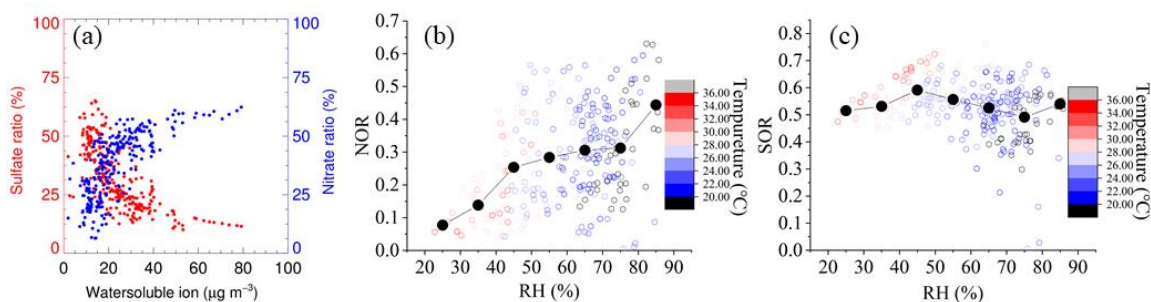
268

269 **Figure 4** (a) Particulate ion mass concentration ratio of nitrate and sulfate to water

270 soluble ion. (b) NOR against RH, colored with temperature. (c) SOR against RH,

271 colored with temperature.

272

To further assess the conversion capacity of nitrate and sulfate in this site, the sulfur oxidation ratio (SOR) and the nitrogen oxidation ratio (NOR) are used to indicate the secondary transformation ratio of SO_2 and NO_2, respectively (Sun et al., 2006). SOR and NOR are estimated using the formulae below:

277

$$SOR = \frac{nSO_4^{2-}}{nSO_4^{2-}+nSO_2} \qquad\qquad Eq7$$

$$NOR = \frac{nNO_3^{-}}{nNO_3^{-}+nNO_2} \qquad\qquad Eq8$$

278 Where n refers to the molar concentration, the higher SOR and NOR represent more
279 oxidation of gaseous species into a secondary aerosol. As depicted in Figure 4 (b-c),
280 NOR rapidly increases at RH < 45 %, remains constant at 45 % < RH < 75 %, and ends
281 with a sharp increase at RH > 75 %. During the study period, not only is the average
282 concentration of NO2 higher among PD but there is also a significant difference
283 between PD and CD NOR. The average values of NOR are 0.32 in PD and 0.25 in CD,
284 respectively, which manifests the more secondary transformation and pollution
285 potential in PD. In contrast, the SOR stays constant at a high value (~ 0.5) during the
286 whole RH scale, which shows a different pattern from previous research (Li et al., 2017;
287 Zheng et al., 2015). One possible explanation is that SO_2 concentration stays low during
288 the whole campaign (4.4 ± 2.4 ppbv on average), and SO_2 oxidation depends on the
289 limit of SO_2 instead of oxidation capability. Meanwhile, the mean SOR in both
290 situations is over 0.5 (0.52 in CD and 0.56 in PD), further supporting the SO_2 limited
291 hypothesis. Besides, Table 2 summarizes NOR and SOR values in YRD. NOR and
292 SOR in this study are similar to values reported in other YRD research (Shu et al., 2019;
293 Zhang et al., 2020b; Qin et al., 2021; Zhao et al., 2022), except values in 2013 (Wang
294 et al., 2016), but higher than north China study (Cao et al., 2017) which emphasize the
295 solid atmospheric oxidation capacity in YRD region.

Table 2 Statistical result of NOR and SOR in YRD

Location and Year	SOR				NOR				References
	Max	Min	Mean	SD	Max	Min	Mean	SD	
Nanjing 2013 Winter	0.42	0.10	0.28	0.11	0.29	0.15	0.21	0.05	
Suzhou 2013 Winter	0.41	0.15	0.27	0.11	0.30	0.06	0.16	0.08	
Lin'an 2013 Winter	0.50	0.19	0.35	0.11	0.24	0.12	0.18	0.05	(Wang et al., 2016)
Hangzhou 2013 Winter	0.30	0.14	0.21	0.06	0.11	0.06	0.09	0.02	
Ningbo 2013 Winter	0.35	0.09	0.21	0.11	0.23	0.03	0.11	0.07	
YRD 2016 Summer	-	-	0.347	-	-	-	0.11	-	(Shu et al., 2019)
YRD 2016 Winter	-	-	0.247	-	-	-	0.15	-	
Nanjing 2019 spring	0.48	0.38	-	-	0.31	0.29	-	-	(Qin et al., 2021)
Changzhou 2019 spring	0.35	0.3	-	-	0.27	0.23	-	-	
Changzhou 2019 Winter	0. 68	0.24	0.35	0.12	0.44	0.13	0.2	0.1	(Zhang et al., 2020b)
Changzhou 2019 Summer	0.16	0.76	0.54	0.1	0.08	0.63	0.28	0.14	This work

3.3 The derivation of N₂O₅ uptake coefficient

Statistical analysis of the observation above highlights the rapid formation of particulate nitrate. To assess the contribution of N_2O_5 hydrolysis to particular nitrate formation, two methods are applied to calculate the N_2O_5 uptake coefficient. The first method is a stationary-state approximation (Brown et al., 2003). By assuming that the rates of production and loss of N_2O_5 are approximately in balance, the total loss rate of N_2O_5 ($k_{N_2O_5}$) can be calculated through equation 9. The $k_{N_2O_5}$ is main dominated by N_2O_5 heterogeneous uptake, since homogeneous hydrolysis of N_2O_5 contribute tiny (Brown and Stutz, 2012). N_2O_5 uptake coefficient through steady-state (note as $\gamma_{\_S}$) is derived as equation 10. Here C is the mean molecule speed of N_2O_5, and S_a is the aerosol surface concentration.

$$\tau_{ss}(N_2O_5) = \frac{[N_2O_5]}{k_{R3.1}[NO_2][O_3]} = (k_{N_2O_5} + \frac{k_{NO_3}}{K_{eq}[NO_2]})^{-1} \qquad \text{Eq9}$$

$$k_{N_2O_5} = 0.25\, C\, \gamma_{\_S}\, S_a \qquad \text{Eq10}$$

Due to the fast variety of NO_3 loss rates from VOCs, the steady-state method has been unattainable in conditions affected by emission interferences. During the whole campaign, we only retrieve three valid fitting results. As shown in Figure 5, the fitted

311 γ_S ranged from 0.057 to 0.123, which is comparable with Taizhou (0.041, Wang et al.

312 (2020a)) and much higher than other results in China (Yu et al., 2020a; Wang et al.,

313 2018a; Wang et al., 2020b; Wang et al., 2017a). The calculated k_{NO_3} ranged from 0.002

314 to 0.16 s^{-1}, represents drastic VOCs change during this campaign.

315
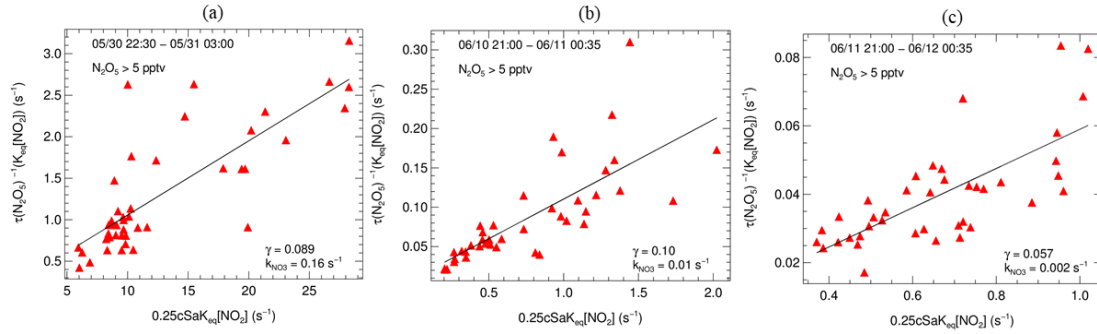
Figure 5 Derived N_2O_5 uptake coefficients from N_2O_5 steady lifetime (γ_S) with NO_2
and S_a, plots (a-c) represent the linear fitting results on the nights of 05/30, 06/10, and
06/11, respectively.

319 The other approach is the parameterization by (Yu et al., 2020a) which is depicted

320 as follows:

$$\gamma_P = \frac{4}{c}\frac{V_a}{S_a}\,K_H \times 3.0 \times 10^4 \times [H_2O]\left(1 - \frac{1}{\left(0.033 \times \frac{[H_2O]}{[NO_3^-]}\right) + 1 + \left(3.4 \times \frac{[Cl^-]}{[NO_3^-]}\right)}\right) \qquad \text{Eq11}$$

321

322 Where V_a/S_a is the measured aerosol volume to surface area ratio by SMPS; K_H is

323 Henry's law coefficient which is set as 51 as recommended; $[NO_3^-]$ and $[Cl^-]$ are aerosol

324 inorganic concentration measured by Marga; $[H_2O]$ is aerosol water content calculated

325 through ISORROPIA II. The valid parameterization calculated N_2O_5 uptake coefficient

326 (note as γ_P) from May 30th to June 08th, 2019, shows in Figure 6 a good consistency

327 between the trends of γ_P and aerosol water content. Nighttime γ_P varies from 0.001 to

328 0.024 with an average of 0.069 ± 0.0050 in polluted condition and 0.0036 ± 0.0026 in

329 clean condition. The N_2O_5 uptake coefficient shows a good correlation between RH and

330 aerosol water content. For the N_2O_5 uptake coefficient, although particulate nitrate mass

331 concentration increased during the pollution event, an antagonistic effect on the N_2O_5

332 uptake coefficient was not obvious for the nitrate molarity decreasing.

333   Furthermore, we compare the difference between γ_S and γ_P[h]. Taking the night of

334   May 30th as an example, the γ_S is 0.089 while γ_P ranges from 0.024 to 0.057 with an

335   average value of 0.013 ± 0.0051. The difference between steady-state and

336   parameterization is significant; one possible explanation is uncertainty for stationary-

337   state approximation caused by local NO or VOCs emission (Brown et al., 2009; Chen

338   et al., 2022). Another reason is that parameterization by Yu et al. ignores the impact of

339   organic matter on the fine particle. The difference in aerosol composition between this

340   work and Yu et al may also bring uncertainty. Overall consideration, γ_P will be chosen

341   for the N_2O_5 heterogeneous uptake coefficient in later analysis and discussion.

342
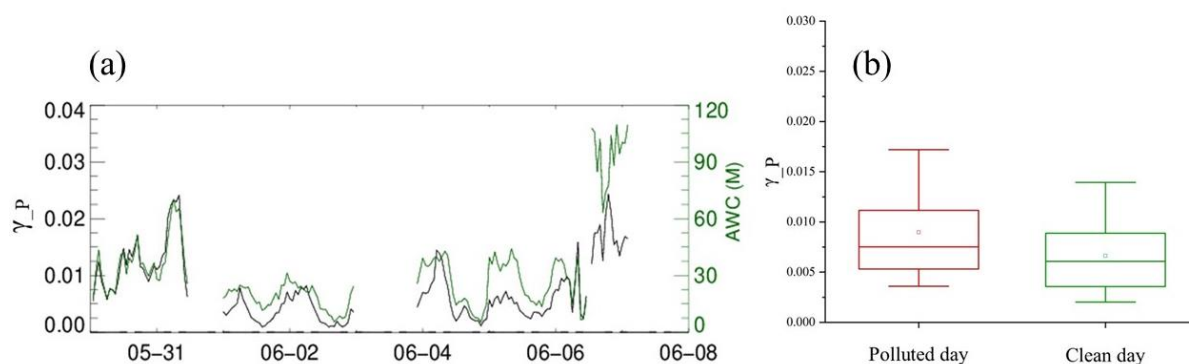
343   **Figure 6** Results of N_2O_5 uptake coefficients through parameterization (γ_p). (a) shows

344   timeseries of γ_p and ISORROPIA II results of aerosol water content (AWC). (b) is the

345   box-plot of γ_p on the polluted day and clean day, the hollow square represents the mean

346   value, and the solid line across the box shows the median score for the data set, while

347   the top and bottom whiskers represent 90 % and 10 % value of γ_p, respectively.

348   **3.4 Quantifying the contribution of nitrate formation pathways**

349   After the N_2O_5 uptake coefficient is counted, nitrate production potential ($P(NO_3^-)$) can

350   be calculated. Here N_2O_5 uptake coefficient is set as 0.036 on clean day and 0.069 on

351   polluted day, respectively, which are the average value derived from parameterization.

352   The production ratio of NO_3^- (by considering $ClNO_2$ yield of 0.54) is set as 1.46 in the

353   former study (Xia et al., 2020). Gas particle distribution is considered by the result of

354   particular nitrate and gas-phase nitrate by MARGA (input HNO_3/NO_3^- ratio to the

355   model as $OH + NO_2$ nitrate production rate). NO_2 heterogeneous uptake coefficient is set

356   as 5.8×10^{-6} depending on the report by Yu et al. (2021) which is the result of 70% RH

357   on urban grime.

358   The mean diurnal variations of the nitrate production potential of clean and polluted

359   day are depicted in Figure 7. The $OH + NO_2$ pathway shows no significate difference

360   between clean and polluted day and dominates clean day nitrate formation potential.

361   Since the level of OH and NO_2 is less affected by the fine particle level. However, the

362   rapid increase of the N_2O_5 heterogeneous uptake pathway on polluted day is fatal, and

363   its peak formation rate at night over the $OH + NO_2$ pathway can be used to explain

364   nighttime nitrate explosive growth.

365   As shown in Figure 7c, $OH + NO_2$ dominates nitrate production on clean day, while

366   the N_2O_5 uptake pathway only contributes 13.6 μg m^{-3}. On polluted days, the ability of

367   N_2O_5 uptake grows fast, reaching 50.1 μg m-3, while the OH pathway doesn't change

368   much. There is no distinct difference in the daytime pathway ($OH + NO_2$) between clean

369   day and polluted day, while the nighttime pathway ratio rises from 38.1 % on clean day

370   to 67.2 % on polluted day.NO_2 heterogeneous uptake increases from 0.93 μg m^{-3} on

371   clean day to 2.0 μg m^{-3} on polluted day, but the contribution proportion does not change

372   obviously. Both the higher N_2O_5 uptake coefficient and higher S_a on polluted day

373   increase the contribution of N_2O_5 hydrolysis on particular nitrate at pollution condition.

374
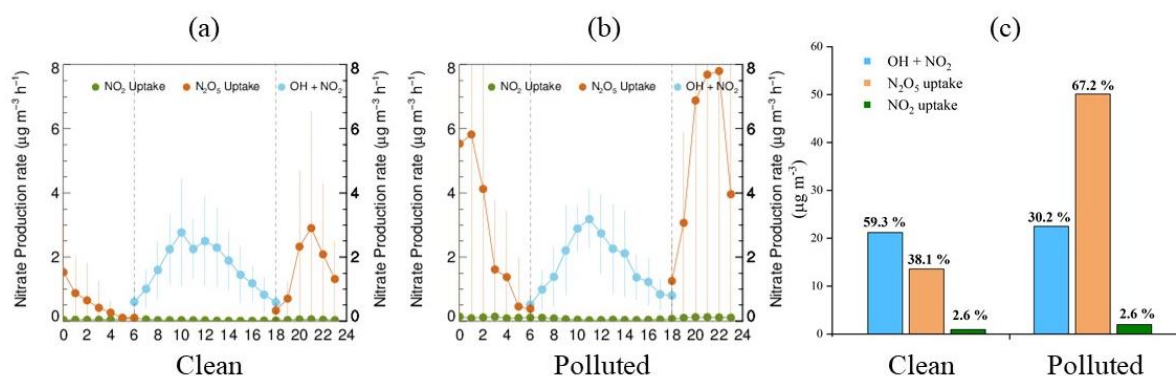
375

376 **Figure 7** The mean diurnal variations of the nitrate production potential of clean day(a)
377 and polluted day (b) and the $P(NO_3^-)$ distribution of clean and polluted day (c).

3.5 Mitigation strategies of particulate nitrate and ozone productions

We selected two pollution episodes (Episode I (2019.05.30 00:00 - 2019.06.02 00:00) and IV (2019.06.14 17:30 - 2019.06.17 12:00)) to explore the mitigation way of ozone and nitrate pollution. Figure 8 shows the EKMA of $P(O_3)$ and $P(NO_3^-)$ of these two periods, O_3 located at VOCs controlling area in the two pollution episodes, which consist with previous YRD urban ozone sensitivity study (Jiang et al., 2018; Zhang et al., 2020a; Xu et al., 2021). The best precursor reduction for O_3 is VOCs: $NO_x = 2:1$ while nitrate is located at the transition area, which means either of the precursors reduction will mitigate nitrate pollution. For the regional and complex air pollution characteristics in this region, a fine particle-targeting reduction scheme will aggravate O_3 pollution. In contrast, the O_3-targeting scheme can mitigate O_3 and fine particle simultaneously.
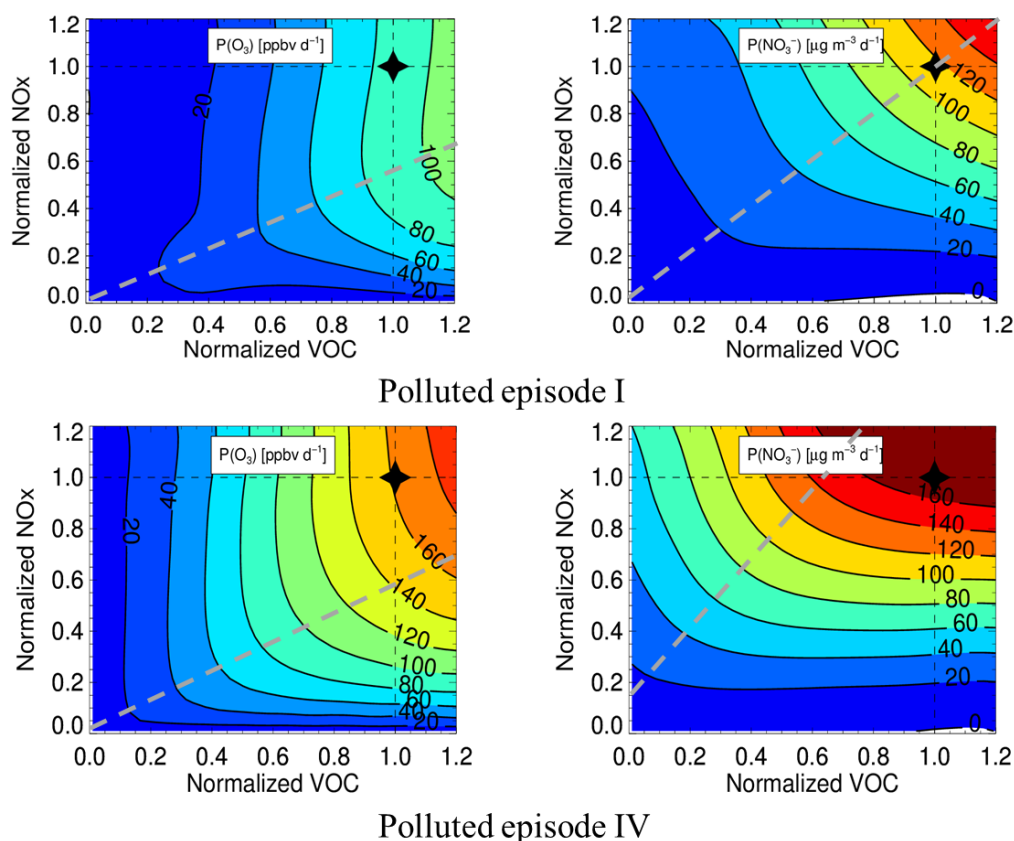
Figure 8 Isogram of $P(O_3)$ and $P(NO_3^-)$ of polluted episode I (2019.05.30 00:00 - 2019.06.02 00:00) and IV (2019.06.14 17:30 - 2019.06.17 12:00) with different NOx and VOC reduction degree. The grey dash line represents the ridge line.

4 Conclusion

A comprehensive campaign was conducted to interpret the atmospheric oxidation capacity and aerosol formation from May 30th to June 18th, 2019, in Changzhou, China. The high O$_3$ and PM$_{2.5}$ concentrations confirm complex air pollution characteristics in Changzhou, and nitrate accounts for 38.3 % mass concentration of total water-soluble particulate components and 32.0 % of total PM$_{2.5}$. In addition, the average values of NOR are 0.32 in PD and 0.25 in CD. The positive correlation between NOR and RH and inverse correlation refer to the contribution of N$_2$O$_5$ heterogeneous uptake to nitrate formation.

Based on field observations of OH and related parameters, we show OH oxidation of the NO$_2$ pathway steadily contributes to nitrate formation no matter the clean or polluted period and domination clean day nitrate production (about 22 μg m^{-3}). N$_2$O$_5$ heterogeneous uptake contribution proliferated on polluted day, from 13.6 μg m^{-3} (38.1 %) on clean days to 50.1 μg m^{-3} (67.2 %) on polluted days. NO$_2$ heterogeneous uptake contributes minor to nitrate formation (2.6 %).

The precursor reduction simulation suggests the reduction ratio of VOCs: NO$_x$ equals 2:1 can simultaneously and effectively mitigate O$_3$ and fine particle pollution during the summertime complex pollution period in Changzhou. To more precisely and delicately establish a cooperative control scheme for regional O$_3$ and nitrate, the regional and long-time field campaigns are needed in the future to analyze the seasonal and interannual variation of O$_3$ and nitrate and relevant parameters.

Code/Data availability. The datasets used in this study are available from the corresponding author upon request (k.lu@pku.edu.cn).

Author contributions. K.D.L. and Y.H.Z. designed the study. T.Y.Z analyzed the data and wrote the paper with input from all authors.

Competing interests. The authors declare that they have no conflicts of interest.

424 **Acknowledgments**. This project is supported by the National Natural Science
425 Foundation of China (21976006); the Beijing Municipal Natural Science Foundation
426 for Distinguished Young Scholars (JQ19031); the National Research Program for Key
427 Issue in Air Pollution Control (DQGG0103-01, 2019YFC0214800). Thanks for the data
428 contributed by field campaign team.

References

430 Andreae, M. O., Schmid, O., Yang, H., Chand, D., Yu, J. Z., Zeng, L.-M., and Zhang,
431   Y.-H.: Optical properties and chemical composition of the atmospheric aerosol in
432   urban Guangzhou, China, Atmospheric Environment, 42, 6335-6350,
433   10.1016/j.atmosenv.2008.01.030, 2008.
434 Bertram, T. H. and Thornton, J. A.: Toward a general parameterization of N2O5
435   reactivity on aqueous particles: the competing effects of particle liquid water,
436   nitrate and chloride, Atmospheric Chemistry and Physics, 9, 8351-8363,
437   10.5194/acp-9-8351-2009, 2009.
438 Bohn, B., Corlett, G. K., Gillmann, M., Sanghavi, S., Stange, G., Tensing, E.,
439   Vrekoussis, M., Bloss, W. J., Clapp, L. J., Kortner, M., Dorn, H. P., Monks, P.
440   S., Platt, U., Plass-Dülmer, C., Mihalopoulos, N., Heard, D. E., Clemitshaw, K.
441   C., Meixner, F. X., Prevot, A. S. H., and Schmitt, R.: Photolysis frequency
442   measurement techniques: results of a comparison within the ACCENT project,
443   ACP, 8, 5373-5391, 10.5194/acp-8-5373-2008, 2008.
444 Brown, S. S. and Stutz, J.: Nighttime radical observations and chemistry, Chemical
445   Society Reviews, 41, 6405-6447, 10.1039/c2cs35181a, 2012.
446 Brown, S. S., Stark, H., and Ravishankara, A. R.: Applicability of the steady state
447   approximation to the interpretation of atmospheric observations of NO3 and
448   N2O5, Journal of Geophysical Research-Atmospheres, 108, 10,
449   10.1029/2003jd003407, 2003.
450 Brown, S. S., Dube, W. P., Fuchs, H., Ryerson, T. B., Wollny, A. G., Brock, C. A.,
451   Bahreini, R., Middlebrook, A. M., Neuman, J. A., Atlas, E., Roberts, J. M.,
452   Osthoff, H. D., Trainer, M., Fehsenfeld, F. C., and Ravishankara, A. R.: Reactive
453   uptake coefficients for N2O5 determined from aircraft measurements during the
454   Second Texas Air Quality Study: Comparison to current model
455   parameterizations, Journal of Geophysical Research-Atmospheres, 114,
456   10.1029/2008jd011679, 2009.
457 Burkholder, J. B., Sander, S. P., Abbatt, J., Barker, J., Huie, R., Kolb, C. E., Kurylo,
458   M., Orkin, V., Wilmouth, D. M., and Wine, P.: Chemical Kinetics and
459   Photochemical Data for Use in Atmospheric Studies, Evaluation Number 18,
460   10.13140/RG.2.1.2504.2806, 2015.
461 Cao, J.-J., Shen, Z.-X., Chow, J. C., Watson, J. G., Lee, S.-C., Tie, X.-X., Ho, K.-F.,
462   Wang, G.-H., and Han, Y.-M.: Winter and Summer PM2.5 Chemical

463   Compositions in Fourteen Chinese Cities, J Air Waste Manage, 62, 1214-1226,
464   10.1080/10962247.2012.701193, 2012.

465 Cao, Z., Zhou, X., Ma, Y., Wang, L., Wu, R., Chen, B., and Wang, W.: The
466   Concentrations, Formations, Relationships and Modeling of Sulfate, Nitrate and
467   Ammonium (SNA) Aerosols over China, Aerosol and Air Quality Research, 17,
468   84-97, 10.4209/aaqr.2016.01.0020, 2017.

469 Chan, Y. C., Evans, M. J., He, P. Z., Holmes, C. D., Jaegle, L., Kasibhatla, P., Liu, X.
470   Y., Sherwen, T., Thornton, J. A., Wang, X., Xie, Z. Q., Zhai, S. T., and
471   Alexander, B.: Heterogeneous Nitrate Production Mechanisms in Intense Haze
472   Events in the North China Plain, Journal of Geophysical Research-Atmospheres,
473   126, 10.1029/2021jd034688, 2021.

474 Chang, Y. H., Zhang, Y. L., Tian, C. G., Zhang, S. C., Ma, X. Y., Cao, F., Liu, X. Y.,
475   Zhang, W. Q., Kuhn, T., and Lehmann, M. F.: Nitrogen isotope fractionation
476   during gas-to-particle conversion of NOx to NO3- in the atmosphere -
477   implications for isotope-based NOx source apportionment, Atmospheric
478   Chemistry and Physics, 18, 11647-11661, 10.5194/acp-18-11647-2018, 2018.

479 Chen, H., Hu, R., Xie, P., Xing, X., Ling, L., Li, Z., Wang, F., Wang, Y., Liu, J., and
480   Liu, W.: A hydroxyl radical detection system using gas expansion and fast gating
481   laser-induced fluorescence techniques, J. Environ. Sci., 65, 190-200,
482   10.1016/j.jes.2017.03.012, 2018.

483 Chen, X., Walker, J. T., and Geron, C.: Chromatography related performance of the
484   Monitor for AeRosols and GAses in ambient air (MARGA): laboratory and
485   field-based evaluation, Atmos. Meas. Tech., 10, 3893-3908, 10.5194/amt-10-
486   3893-2017, 2017.

487 Chen, X., Wang, H., and Lu, K.: Interpretation of NO3-N2O5 observation via steady
488   state in high-aerosol air mass: the impact of equilibrium coefficient in ambient
489   conditions, Atmospheric Chemistry and Physics, 22, 3525-3533, 10.5194/acp-
490   22-3525-2022, 2022.

491 Chen, X. R., Wang, H. C., Liu, Y. H., Su, R., Wang, H. L., Lou, S. R., and Lu, K. D.:
492   Spatial characteristics of the nighttime oxidation capacity in the Yangtze River
493   Delta, China, Atmospheric Environment, 208, 150-157,
494   10.1016/j.atmosenv.2019.04.012, 2019.

495 Chen, X. R., Wang, H. C., Lu, K. D., Li, C. M., Zhai, T. Y., Tan, Z. F., Ma, X. F.,
496   Yang, X. P., Liu, Y. H., Chen, S. Y., Dong, H. B., Li, X., Wu, Z. J., Hu, M.,
497   Zeng, L. M., and Zhang, Y. H.: Field Determination of Nitrate Formation
498   Pathway in Winter Beijing, Environmental Science & Technology, 54, 9243-
499   9253, 10.1021/acs.est.0c00972, 2020.

500 Elshorbany, Y. F., Steil, B., Brühl, C., and Lelieveld, J.: Impact of HONO on global
501   atmospheric chemistry calculated with an empirical parameterization in the
502   EMAC model, ACP, 12, 9977-10000, 10.5194/acp-12-9977-2012, 2012.

503 Fountoukis, C. and Nenes, A.: ISORROPIA II: a computationally efficient
504   thermodynamic equilibrium model for K+-Ca2+-Mg2+-Nh(4)(+)-Na+-SO42--

NO3--Cl--H2O aerosols, Atmospheric Chemistry and Physics, 7, 4639-4659, 2007.

Goliff, W. S., Stockwell, W. R., and Lawson, C. V.: The regional atmospheric chemistry mechanism, version 2, Atmospheric Environment, 68, 174-185, 10.1016/j.atmosenv.2012.11.038, 2013.

Guo, L., Hu, Y., Hu, Q., Lin, J., Li, C., Chen, J., Li, L., and Fu, H.: Characteristics and chemical compositions of particulate matter collected at the selected metro stations of Shanghai, China, Science of the Total Environment, 496, 443-452, 10.1016/j.scitotenv.2014.07.055, 2014.

Hagler, G. S. W., Bergin, M. H., Salmon, L. G., Yu, J. Z., Wan, E. C. H., Zheng, M., Zeng, L. M., Kiang, C. S., Zhang, Y. H., Lau, A. K. H., and Schauer, J. J.: Source areas and chemical composition of fine particulate matter in the Pearl River Delta region of China, Atmos. Environ., 40, 3802-3815, 10.1016/j.atmosenv.2006.02.032, 2006.

Jiang, M., Lu, K., Su, R., Tan, Z., Wang, H., Li, L., Fu, Q., Zhai, C., Tan, Q., Yue, D., Chen, D., Wang, Z., Xie, S., Zeng, L., and Zhang, Y.: Ozone formation and key VOCs in typical Chinese city clusters, Chinese Sci Bull, 63, 1130-1141, 2018.

Kanaya, Y., Fukuda, M., Akimoto, H., Takegawa, N., Komazaki, Y., Yokouchi, Y., Koike, M., and Kondo, Y.: Urban photochemistry in central Tokyo: 2. Rates and regimes of oxidant (O-3+NO2) production, Journal of Geophysical Research-Atmospheres, 113, 10.1029/2007jd008671, 2008.

Li, H. Y., Zhang, Q., Zhang, Q., Chen, C. R., Wang, L. T., Wei, Z., Zhou, S., Parworth, C., Zheng, B., Canonaco, F., Prevot, A. S. H., Chen, P., Zhang, H. L., Wallington, T. J., and He, K. B.: Wintertime aerosol chemistry and haze evolution in an extremely polluted city of the North China Plain: significant contribution from coal and biomass combustion, Atmospheric Chemistry and Physics, 17, 4751-4768, 2017.

Liu, X., Gu, J., Li, Y., Cheng, Y., Qu, Y., Han, T., Wang, J., Tian, H., Chen, J., and Zhang, Y.: Increase of aerosol scattering by hygroscopic growth: Observation, modeling, and implications on visibility, Atmos. Res., 132-133, 91-101, https://doi.org/10.1016/j.atmosres.2013.04.007, 2013.

Lou, S., Tan, Z., Gan, G., Chen, J., Wang, H., Gao, Y., Huang, D., Huang, C., Li, X., Song, R., Wang, H., Wang, M., Wang, Q., Wu, Y., and Huang, C.: Observation based study on atmospheric oxidation capacity in Shanghai during late-autumn: Contribution from nitryl chloride, Atmospheric Environment, 271, 118902, https://doi.org/10.1016/j.atmosenv.2021.118902, 2022.

Lu, K. D., Hofzumahaus, A., Holland, F., Bohn, B., Brauers, T., Fuchs, H., Hu, M., Haseler, R., Kita, K., Kondo, Y., Li, X., Lou, S. R., Oebel, A., Shao, M., Zeng, L. M., Wahner, A., Zhu, T., Zhang, Y. H., and Rohrer, F.: Missing OH source in a suburban environment near Beijing: observed and modelled OH and HO2 concentrations in summer 2006, Atmospheric Chemistry and Physics, 13, 1057-1080, 10.5194/acp-13-1057-2013, 2013.

Lu, K. D., Rohrer, F., Holland, F., Fuchs, H., Bohn, B., Brauers, T., Chang, C. C., Haseler, R., Hu, M., Kita, K., Kondo, Y., Li, X., Lou, S. R., Nehr, S., Shao, M., Zeng, L. M., Wahner, A., Zhang, Y. H., and Hofzumahaus, A.: Observation and modelling of OH and HO2 concentrations in the Pearl River Delta 2006: a missing OH source in a VOC rich atmosphere, Atmospheric Chemistry and Physics, 12, 1541-1569, 10.5194/acp-12-1541-2012, 2012.

Ma, X. F., Tan, Z. F., Lu, K. D., Yang, X. P., Chen, X. R., Wang, H. C., Chen, S. Y., Fang, X., Li, S. L., Li, X., Liu, J. W., Liu, Y., Lou, S. R., Qiu, W. Y., Wang, H. L., Zeng, L. M., and Zhang, Y. H.: OH and HO2 radical chemistry at a suburban site during the EXPLORE-YRD campaign in 2018, Atmospheric Chemistry and Physics, 22, 7005-7028, 2022.

Meng, Z. Y., Wu, L. Y., Xu, X. D., Xu, W. Y., Zhang, R. J., Jia, X. F., Liang, L. L., Miao, Y. C., Cheng, H. B., Xie, Y. L., He, J. J., and Zhong, J. T.: Changes in ammonia and its effects on PM2.5 chemical property in three winter seasons in Beijing, China, Science of the Total Environment, 749, 2020.

Ming, L., Jin, L., Li, J., Fu, P., Yang, W., Liu, D., Zhang, G., Wang, Z., and Li, X.: PM2.5 in the Yangtze River Delta, China: Chemical compositions, seasonal variations, and regional pollution events, Environmental Pollution, 223, 200-212, 10.1016/j.envpol.2017.01.013, 2017.

Phillips, G. J., Thieser, J., Tang, M. J., Sobanski, N., Schuster, G., Fachinger, J., Drewnick, F., Borrmann, S., Bingemer, H., Lelieveld, J., and Crowley, J. N.: Estimating N2O5 uptake coefficients using ambient measurements of NO3, N2O5, ClNO2 and particle-phase nitrate, Atmospheric Chemistry and Physics, 16, 13231-13249, 10.5194/acp-16-13231-2016, 2016.

Qin, Y., Li, J. Y., Gong, K. J., Wu, Z. J., Chen, M. D., Qin, M. M., Huang, L., and Hu, J. L.: Double high pollution events in the Yangtze River Delta from 2015 to 2019: Characteristics, trends, and meteorological situations, Science of the Total Environment, 792, 10.1016/j.scitotenv.2021.148349, 2021.

Qiu, X. H., Ying, Q., Wang, S. X., Duan, L., Zhao, J., Xing, J., Ding, D., Sun, Y. L., Liu, B. X., Shi, A. J., Yan, X., Xu, Q. C., and Hao, J. M.: Modeling the impact of heterogeneous reactions of chlorine on summertime nitrate formation in Beijing, China, Atmospheric Chemistry and Physics, 19, 6737-6747, 10.5194/acp-19-6737-2019, 2019.

Seinfeld, J. H. and Pandis, S. N.: Atmospheric chemistry and physics: from air pollution to climate change, Third;3rd;, Book, Whole, Wiley, Hoboken, New Jersey2016.

Shang, D. J., Peng, J. F., Guo, S., Wu, Z. J., and Hu, M.: Secondary aerosol formation in winter haze over the Beijing-Tianjin-Hebei Region, China, Front. Env. Sci. Eng., 15, 13, 10.1007/s11783-020-1326-x, 2021.

Shu, L., Wang, T. J., Xie, M., Li, M. M., Zhao, M., Zhang, M., and Zhao, X. Y.: Episode study of fine particle and ozone during the CAPUM-YRD over Yangtze River Delta of China: Characteristics and source attribution, Atmospheric

Environment, 203, 87-101, 10.1016/j.atmosenv.2019.01.044, 2019.

Song, C. H. and Carmichael, G. R.: Gas-particle partitioning of nitric acid modulated by alkaline aerosol, Journal of Atmospheric Chemistry, 40, 1-22, 2001.

Staudt, S., Gord, J. R., Karimova, N. V., McDuffie, E. E., Brown, S. S., Gerber, R. B., Nathanson, G. M., and Bertram, T. H.: Sulfate and Carboxylate Suppress the Formation of ClNO2 at Atmospheric Interfaces, Acs Earth and Space Chemistry, 3, 1987-1997, 2019.

Sun, Y. L., Zhuang, G. S., Tang, A. H., Wang, Y., and An, Z. S.: Chemical characteristics of PM2.5 and PM10 in haze-fog episodes in Beijing, Environmental Science & Technology, 40, 3148-3155, 10.1021/es051533g, 2006.

Tan, Z., Wang, H., Lu, K., Dong, H., Liu, Y., Zeng, L., Hu, M., and Zhang, Y.: An Observational Based Modeling of the Surface Layer Particulate Nitrate in the North China Plain During Summertime, Journal of Geophysical Research: Atmospheres, 126, e2021JD035623, https://doi.org/10.1029/2021JD035623, 2021.

Tan, Z. F., Lu, K. D., Dong, H. B., Hu, M., Li, X., Liu, Y. H., Lu, S. H., Shao, M., Su, R., Wang, H. C., Wu, Y. S., Wahner, A., and Zhang, Y. H.: Explicit diagnosis of the local ozone production rate and the ozone-NOx-VOC sensitivities, Science Bulletin, 63, 1067-1076, 10.1016/j.scib.2018.07.001, 2018.

Tan, Z. F., Fuchs, H., Lu, K. D., Hofzumahaus, A., Bohn, B., Broch, S., Dong, H. B., Gomm, S., Haseler, R., He, L. Y., Holland, F., Li, X., Liu, Y., Lu, S. H., Rohrer, F., Shao, M., Wang, B. L., Wang, M., Wu, Y. S., Zeng, L. M., Zhang, Y. S., Wahner, A., and Zhang, Y. H.: Radical chemistry at a rural site (Wangdu) in the North China Plain: observation and model calculations of OH, HO2 and RO2 radicals, Atmospheric Chemistry and Physics, 17, 663-690, 10.5194/acp-17-663-2017, 2017.

Tham, Y. J., Wang, Z., Li, Q., Wang, W., Wang, X., Lu, K., Ma, N., Yan, C., Kecorius, S., Wiedensohler, A., Zhang, Y., and Wang, T.: Heterogeneous N2O5 uptake coefficient and production yield of ClNO2 in polluted northern China: roles of aerosol water content and chemical composition, Atmospheric Chemistry and Physics, 18, 13155-13171, 10.5194/acp-18-13155-2018, 2018.

Wang, H., Zhu, B., Shen, L., Xu, H., An, J., Pan, C., Li, Y. e., and Liu, D.: Regional Characteristics of Air Pollutants during Heavy Haze Events in the Yangtze River Delta, China, Aerosol and Air Quality Research, 16, 2159-2171, 10.4209/aaqr.2015.09.0551, 2016.

Wang, H., Lu, K., Chen, X., Zhu, Q., Chen, Q., Guo, S., Jiang, M., Li, X., Shang, D., Tan, Z., Wu, Y., Wu, Z., Zou, Q., Zheng, Y., Zeng, L., Zhu, T., Hu, M., and Zhang, Y.: High N2O5 Concentrations Observed in Urban Beijing: Implications of a Large Nitrate Formation Pathway, Environmental Science and Technology Letters, 4, 416-420, 10.1021/acs.estlett.7b00341, 2017a.

Wang, H. C. and Lu, K. D.: Determination and Parameterization of the Heterogeneous

Uptake Coefficient of Dinitrogen Pentoxide (N2O5), Prog. Chem., 28, 917-933, 10.7536/pc151225, 2016.

Wang, H. C., Chen, J., and Lu, K. D.: Development of a portable cavity-enhanced absorption spectrometer for the measurement of ambient NO3 and N2O5: experimental setup, lab characterizations, and field applications in a polluted urban environment, Atmos. Meas. Tech., 10, 1465-1479, 10.5194/amt-10-1465-2017, 2017b.

Wang, H. C., Lu, K. D., Chen, X. R., Zhu, Q. D., Wu, Z. J., Wu, Y. S., and Sun, K.: Fast particulate nitrate formation via N2O5 uptake aloft in winter in Beijing, Atmospheric Chemistry and Physics, 18, 10483-10495, 10.5194/acp-18-10483-2018, 2018a.

Wang, H. C., Chen, X. R., Lu, K. D., Hu, R. Z., Li, Z. Y., Wang, H. L., Ma, X. F., Yang, X. P., Chen, S. Y., Dong, H. B., Liu, Y., Fang, X., Zeng, L. M., Hu, M., and Zhang, Y. H.: NO3 and N2O5 chemistry at a suburban site during the EXPLORE-YRD campaign in 2018, Atmospheric Environment, 224, 9, 10.1016/j.atmosenv.2019.117180, 2020a.

Wang, H. C., Chen, X. R., Lu, K. D., Tan, Z. F., Ma, X. F., Wu, Z. J., Li, X., Liu, Y. H., Shang, D. J., Wu, Y. S., Zeng, L. M., Hu, M., Schmitt, S., Kiendler-Scharr, A., Wahner, A., and Zhang, Y. H.: Wintertime N2O5 uptake coefficients over the North China Plain, Science Bulletin, 65, 765-774, 10.1016/j.scib.2020.02.006, 2020b.

Wang, H. C., Lu, K. D., Guo, S., Wu, Z. J., Shang, D. J., Tan, Z. F., Wang, Y. J., Le Breton, M., Lou, S. R., Tang, M. J., Wu, Y. S., Zhu, W. F., Zheng, J., Zeng, L. M., Hallquist, M., Hu, M., and Zhang, Y. H.: Efficient N2O5 uptake and NO3 oxidation in the outflow of urban Beijing, Atmospheric Chemistry and Physics, 18, 9705-9721, 10.5194/acp-18-9705-2018, 2018b.

Wang, S. B., Wang, L. L., Fan, X. G., Wang, N., Ma, S. L., and Zhang, R. Q.: Formation pathway of secondary inorganic aerosol and its influencing factors in Northern China: Comparison between urban and rural sites, Science of the Total Environment, 840, 2022.

Wang, X. F., Zhang, Y. P., Chen, H., Yang, X., Chen, J. M., and Geng, F. H.: Particulate Nitrate Formation in a Highly Polluted Urban Area: A Case Study by Single-Particle Mass Spectrometry in Shanghai, Environmental Science & Technology, 43, 3061-3066, 2009.

Wang, Z., Wang, W. H., Tham, Y. J., Li, Q. Y., Wang, H., Wen, L., Wang, X. F., and Wang, T.: Fast heterogeneous N2O5 uptake and ClNO2 production in power plant and industrial plumes observed in the nocturnal residual layer over the North China Plain, Atmospheric Chemistry and Physics, 17, 12361-12378, 10.5194/acp-17-12361-2017, 2017c.

Woodward-Massey, R., Slater, E. J., Alen, J., Ingham, T., Cryer, D. R., Stimpson, L. M., Ye, C. X., Seakins, P. W., Whalley, L. K., and Heard, D. E.: Implementation of a chemical background method for atmospheric OH measurements by laser-

induced fluorescence: characterisation and observations from the UK and China, Atmos. Meas. Tech., 13, 3119-3146, 10.5194/amt-13-3119-2020, 2020.

Wu, S. P., Dai, L. H., Zhu, H., Zhang, N., Yan, J. P., Schwab, J. J., and Yuan, C. S.: The impact of sea-salt aerosols on particulate inorganic nitrogen deposition in the western Taiwan Strait region, China, Atmos. Res., 228, 68-76, 2019.

Xia, M., Peng, X., Wang, W., Yu, C., Sun, P., Li, Y., Liu, Y., Xu, Z., Wang, Z., Xu, Z., Nie, W., Ding, A., and Wang, T.: Significant production of $ClNO_2$ and possible source of Cl-2 from N_2O_5 uptake at a suburban site in eastern China, Atmospheric Chemistry and Physics, 20, 6147-6158, 10.5194/acp-20-6147-2020, 2020.

Xu, J. W., Huang, X., Wang, N., Li, Y. Y., and Ding, A. J.: Understanding ozone pollution in the Yangtze River Delta of eastern China from the perspective of diurnal cycles, Science of the Total Environment, 752, 10.1016/j.scitotenv.2020.141928, 2021.

Xue, H., Liu, G., Zhang, H., Hu, R., and Wang, X.: Similarities and differences in PM10 and PM2.5 concentrations, chemical compositions and sources in Hefei City, China, Chemosphere, 220, 760-765, 10.1016/j.chemosphere.2018.12.123, 2019.

Yang, X. P., Lu, K. D., Ma, X. F., Liu, Y. H., Wang, H. C., Hu, R. Z., Li, X., Lou, S. R., Chen, S. Y., Dong, H. B., Wang, F. Y., Wang, Y. H., Zhang, G. X., Li, S. L., Yang, S. D., Yang, Y. M., Kuang, C. L., Tan, Z. F., Chen, X. R., Qiu, P. P., Zeng, L. M., Xie, P. H., and Zhang, Y. H.: Observations and modeling of OH and HO_2 radicals in Chengdu, China in summer 2019, Science of the Total Environment, 772, 2021.

Yu, C., Wang, Z., Xia, M., Fu, X., Wang, W. H., Tham, Y. J., Chen, T. S., Zheng, P. G., Li, H. Y., Shan, Y., Wang, X. F., Xue, L. K., Zhou, Y., Yue, D. L., Ou, Y. B., Gao, J., Lu, K. D., Brown, S. S., Zhang, Y. H., and Wang, T.: Heterogeneous N_2O_5 reactions on atmospheric aerosols at four Chinese sites: improving model representation of uptake parameters, Atmospheric Chemistry and Physics, 20, 4367-4378, 10.5194/acp-20-4367-2020, 2020a.

Yu, C. A., Wang, Z., Ma, Q. X., Xue, L. K., George, C., and Wang, T.: Measurement of heterogeneous uptake of NO_2 on inorganic particles, sea water and urban grime, J. Environ. Sci., 106, 124-135, 10.1016/j.jes.2021.01.018, 2021.

Yu, D., Tan, Z., Lu, K., Ma, X., Li, X., Chen, S., Zhu, B., Lin, L., Li, Y., Qiu, P., Yang, X., Liu, Y., Wang, H., He, L., Huang, X., and Zhang, Y.: An explicit study of local ozone budget and NOx-VOCs sensitivity in Shenzhen China, Atmospheric Environment, 224, 117304, 10.1016/j.atmosenv.2020.117304, 2020b.

Zhang, K., Xu, J. L., Huang, Q., Zhou, L., Fu, Q. Y., Duan, Y. S., and Xiu, G. L.: Precursors and potential sources of ground-level ozone in suburban Shanghai, Front. Env. Sci. Eng., 14, 10.1007/s11783-020-1271-8, 2020a.

Zhang, R., Han, Y. H., Shi, A. J., Sun, X. S., Yan, X., Huang, Y. H., and Wang, Y.:

Characteristics of ambient ammonia and its effects on particulate ammonium in winter of urban Beijing, China, Environ Sci Pollut R, 28, 62828-62838, 2021.

Zhang, Y., Hong, Z., Chen, J., Xu, L., Hong, Y., Li, M., Hao, H., Chen, Y., Qiu, Y., Wu, X., Li, J.-R., Tong, L., and Xiao, H.: Impact of control measures and typhoon weather on characteristics and formation of PM2.5 during the 2016 G20 summit in China, Atmospheric Environment, 224, 117312, https://doi.org/10.1016/j.atmosenv.2020.117312, 2020b.

Zhang, Y., Tang, L., Yu, H., Wang, Z., Sun, Y., Qin, W., Chen, W., Chen, C., Ding, A., Wu, J., Ge, S., Chen, C., and Zhou, H.-c.: Chemical composition, sources and evolution processes of aerosol at an urban site in Yangtze River Delta, China during wintertime, Atmospheric Environment, 123, 339-349, 10.1016/j.atmosenv.2015.08.017, 2015.

Zhang, Y., Tang, L., Croteau, P. L., Favez, O., Sun, Y., Canagaratna, M. R., Wang, Z., Couvidat, F., Albinet, A., Zhang, H., Sciare, J., Prevot, A. S. H., Jayne, J. T., and Worsnop, D. R.: Field characterization of the PM2.5 Aerosol Chemical Speciation Monitor: insights into the composition, sources, and processes of fine particles in eastern China, Atmospheric Chemistry and Physics, 17, 14501-14517, 10.5194/acp-17-14501-2017, 2017.

Zhang, Y. Y., Tang, A. H., Wang, C., Ma, X., Li, Y. Z., Xu, W., Xia, X. P., Zheng, A. H., Li, W. Q., Fang, Z. G., Zhao, X. F., Peng, X. L., Zhang, Y. P., Han, J., Zhang, L. J., Collett, J. L., and Liu, X. J.: PM (2.5) and water-soluble inorganic ion concentrations decreased faster in urban than rural areas in China, J. Environ. Sci., 122, 83-91, 2022.

Zhao, P. S., Dong, F., He, D., Zhao, X. J., Zhang, X. L., Zhang, W. Z., Yao, Q., and Liu, H. Y.: Characteristics of concentrations and chemical compositions for PM2.5 in the region of Beijing, Tianjin, and Hebei, China, Atmospheric Chemistry and Physics, 13, 4631-4644, 10.5194/acp-13-4631-2013, 2013.

Zhao, Z. Z., Sun, N., Zhou, W. L., Ma, S. S., Li, X. D., Li, M. L., Zhang, X., Tang, S. S., and Ye, Z. L.: Chemical Compositions in Winter PM2.5 in Changzhou of the Yangtze River Delta Region, China: Characteristics and Atmospheric Responses Along With the Different Pollution Levels, Front Env Sci-Switz, 10, 2022.

Zheng, G. J., Duan, F. K., Su, H., Ma, Y. L., Cheng, Y., Zheng, B., Zhang, Q., Huang, T., Kimoto, T., Chang, D., Poschl, U., Cheng, Y. F., and He, K. B.: Exploring the severe winter haze in Beijing: the impact of synoptic weather, regional transport and heterogeneous reactions, Atmospheric Chemistry and Physics, 15, 2969-2983, 2015.